Desalination and Water Treatment
www.deswater.com

doi: 10.5004/dwt.2020.25800

193 (2020) 212–223
July

Exergoeconomic and environmental analysis of a combined power and water desalination plant with parabolic solar collector

Mohammad Amin Javadi[a], Mehdi Khalaji[a], Ramin Ghasemiasl[b,*]

[a]*Young Researchers and Elite Club, West Tehran Branch, Islamic Azad University, Tehran, Iran, Tel. +98–912-661-4562; email: benyaminjava@gmail.com (M.A. Javadi), Tel. +98-919-465-1907; email: khalaji.mehdi89@gmail.com (M. Khalaji)*
[b]*Department of Mechanical Engineering, West Tehran Branch, Islamic Azad University, Tehran, Iran, Tel. +98-912-206-6068; email: info@ghasemiasl.ir (R. Ghasemiasl)*

Received 25 August 2019; Accepted 8 March 2020

ABSTRACT

In this research, Abadan combined cycle power plant (CCPP) has been thermodynamically modeled and the obtained results have been compared with the information obtained from the design conditions of the system. By introducing a multi-effect desalination cycle and several parabolic solar collectors, the CCPP, and the effects of these changes on its performance have been investigated. In this study, the exergy efficiency, carbon dioxide emission, and the cost of electricity generation have been considered based on the SPECO model. The results show that the thermal and exergy efficiency of the cogeneration of power and water with the parabolic solar collectors (CPWSC) depends on the design parameters. The efficiency of the power plant after using multi effect desalination (MED) system and parabolic solar collector increases from 48.71% to 50.91% and the exergy efficiency enhances from 45.95 to 50.03. The heat loss in the steam cycle is reduced by 29%. Also, a reduction in the cost of exergy destruction in the condenser is observed to be 13.56%. The CPWSC produces 20,000 tons of freshwater per day. Also, CO_2 emissions have decreased from 58.05 to 54.97 kg per megawatt hour of electricity.

Keywords: Combined cycle; Exergy efficiency; Exergy destruction; Environmental effects; Cogeneration plant; Multi effect desalination; Parabolic solar collector

1. Introduction

Nowadays, renewable energies have many applications [1], especially solar energy [2–5]. Their applications are interesting in power generation and water desalination cycles. The latest studies have considered environmental and economic features of integrated power and water desalination cycle but most of the proposed configurations aren't applicable or they require huge investment costs to use in existing power plants. The present study proposes a new configuration for a thermal system that can be implemented in existing power plants. This thermal system is considered that with minor modifications to existing power plants, by adding parabolic solar collectors and multi effect desalination (MED) system can increase overall cycle efficiency in addition to freshwater production from seawater. Finally, a comprehensive investigation including 4E (energy, exergy, economic, environmental) analysis has been carried out on the proposed configuration.

Al Mutaz and Wazeer [6] have studied the effects of performance and important variables on the efficiency of combined cycle power plant (CCPP) with MED-TVC system. These variables include the number of effects, the vapor pressure of the stimulus, the high temperature of the salt, the temperature difference between the effects, and the water supply temperature. They have provided a mathematical model for plant analysis and compared the parameters

* Corresponding author.

with existing power plants data and validated their mathematical model in this way.

Baghernejad and Yaghoubi [7] investigated the Yazd cycle power plant with a solar collector in terms of energy and exergy. The exergy destruction of the power plant has been calculated. Exergy destruction of this power plant due to combustion chamber, solar collector, heat exchangers, pumps, and turbines were 29.62%, 8.69%, 9.11%, 8% of the total exergy input to the power plant and energy efficiency and exergy of 46.17% and 45.6% have been reported, respectively which is greater than the energy and exergy efficiency without solar collector. In another study, they also studied a power, refrigeration, and heat cogeneration plant which reduced the cost of fuel and exergy degradation and environmental impacts by 24.17%, 38.87%, and 24.17%, respectively [8].

Sanjay et al. [9] investigated this type of power plant. The closed-loop-steam-cooling can improve thermal efficiency by up to 62%. In their study, it is shown that the compressor pressure ratio range is a fundamental parameter for improving thermal efficiency. The pressure reheat parameter is another important design parameter for increasing efficiency. With the analysis of exergy, it was found that the highest losses in this cycle are related to the combustion chamber with 30% of losses and then the turbine with the 4% has the highest losses.

Ihm et al. [10] compared the three MSF, MED, and SWRO systems. The result of their investigation includes a comparison between the energy savings in the combination of oil-fired power plant (OFPP) with CCPP. The results show that the amount of energy needed for desalination is 11%–49% lower than that of the OFPP due to the high efficiency of the CCPP.

Si et al. [11] evaluated the exergy of a 1,000 MW double reheat ultra-supercritical power plant. Their results show that the thermal recovery system is associated with a 2.3% of exergy loss. Also, 85% of the exergy loss of the power plant is due to energy losses in the combustion chamber and heat exchangers.

Abuelnuo et al. [12] conducted an exergy assessment for the 180 MW CCPP in Sudan. The results of this study also show that the highest exergy destruction has occurred in the combustion chamber and this is because of the high irreversibility of the combustion process. Sixty-three percent of destructive exergy is as follows: 13.6% gas turbine, 6.4% steam turbine, 6.3% recovery boiler, 4.7% recovery boiler gas, 3.8 compressor, 2% cooling system. There are several methods and approaches in thermo-economism that are theory of exergetic cost [13], theory of exergetic cost disaggregating methodology [14], thermo-economic function analysis [15], intelligent functional approach [16], the last-inside-first-outside principle [17], the specific exergy costing (SPECO) [18] and the engineering functional analysis [19,20].

In this research, the thermodynamic, exergy, economic model of Abadan CCPP was first modeled. The SPECO approach has been used in this research to compare with other studies. Then, the effects of adding MED system and parabolic solar collectors to Abadan CCPP have been investigated and evaluated in terms of exergy, energy, economy, and environment. In this way, the thermal and exergy efficiency, the cost of electricity and water generation, and the pollution are analyzed. An MED system and a parabolic solar collector have been added to the cycle to increase the efficiency of this plant. The cost of investment and the cost of exergy destruction and CO_2 generation have also been investigated. By this method, the losses of various components of the co-generation of electricity and water with parabolic solar collector and costs have been analyzed and compared with Abadan CCPP.

2. Material and method

Abadan power plant with a nominal capacity of 450 MW has been studied in this research according to Fig. 1 and with the design specifications of the system presented in Table 1. Also, a MED system and a parabolic solar collector unit have been added according to Fig. 2.

In this proposed cycle, the compressor outlet air enters the combustion chamber. The exhaust gases from the combustion chamber, upon expanding in the turbine, create thrust, and generates electricity through the gas turbine. The exhaust gases, after passing through the turbine section, enter the dual-pressure heat recovery steam generator (HRSG) and its temperature increased by the duct burner. These exhaust gases are used to produce the energy needed for the Rankine cycle steam turbine (ST). To increase the efficiency of the ST cycle, some of the water used in the high-pressure section of the HRSG is converted to steam by parabolic solar collectors and then transferred to the ST bypasses of the high-pressure superheater heat exchanger. Finally, the steam inlet to ST after going through several stages of the turbine by reducing its pressure will be used as the steam generator for the MED system.

The following hypotheses have been considered in order to model the cogeneration of power and water with the parabolic solar collectors (CPWSC) [21]. All processes in this research are considered to be stable. The air and exhaust gases from the combustion chamber are considered to be ideal gas. The kinetic and potential energy and exergy changes have been neglected. The dead state in this research is T_0 = 299.15 K and P_0 = 1 bar. The pressure drop in the combustion chamber is assumed to be 0.03 Kpa, and in the turbine, compressor and feedwater pump are assumed to be adiabatic. The ambient temperature and pressure have been considered as input into the compressor. The fuel used in this study is methane. The steam formed in each effect is salt-free and the mass flow rate of all the effects is equal. Fig. 2 shows a schematic of the CPWSC.

The economic exergy analysis is linked to the cost associated with the exergy of each streamline. Therefore, in order to analyze the economic exergy, the exergy rate of each of the input and output lines to the various components should be specified. The flow exergy rate is determined at different points of the CPWSC by applying mass, energy, and exergy balance equations. The mass, energy, and exergy balance equations for various components of CPWSC can be calculated for them by considering the control volume specified in Fig. 3 by the following equations [22]:

$$\sum_i \dot{m}_i h_i + \dot{Q} = \sum_e \dot{m}_e h_e + \dot{W} \quad (1)$$

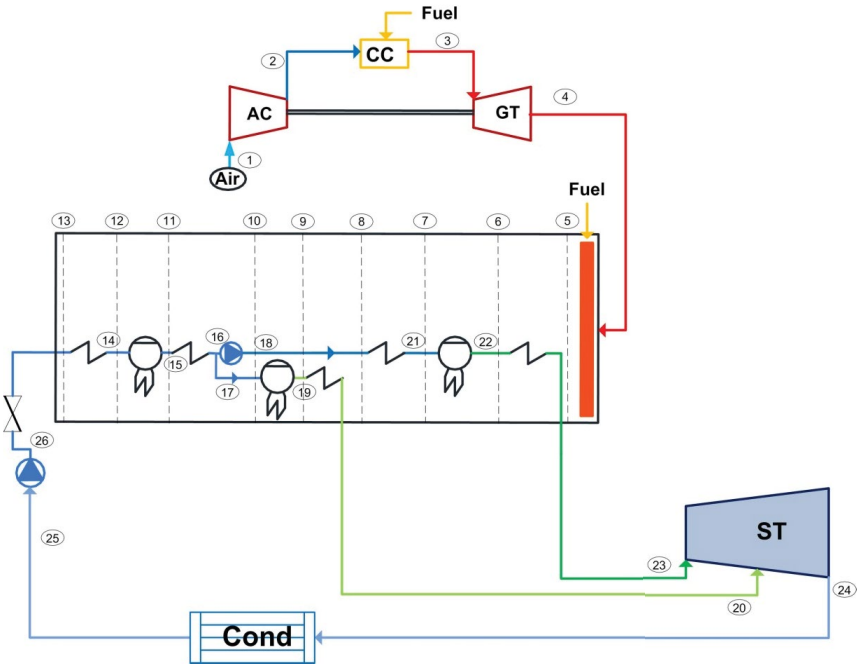

Fig. 1. Schematic of Abadan power plant.

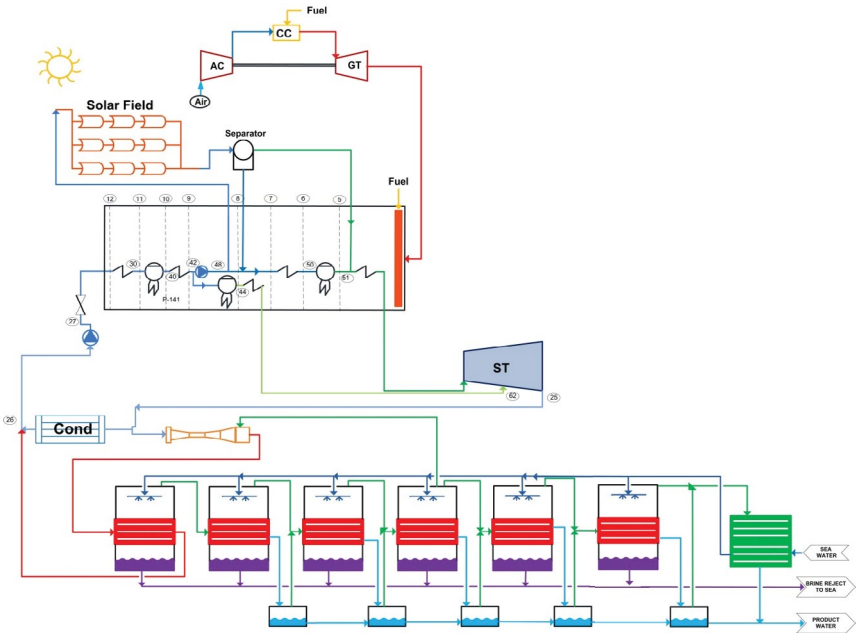

Fig. 2. Schematic of the CPWSC.

$$\dot{E}x_Q + \sum_i \dot{m}_i ex_i = \sum_e \dot{m}_e ex_e + \dot{E}x_W + \dot{E}x_D \quad (2)$$

The chemical exergy of fuel is derived from Eq. (3) [23,24]:

$$\xi = \frac{ex_f}{LHV_f} \quad (3)$$

The result of the division of the chemical exergy of the fuel (methane gas) by LHV_f is usually close to one for gas fuels [25–30]:

$$\xi_{H_2} = 0.985, \xi_{CH_4} = 1.06 \quad (4)$$

The thermo-economic calculations of each system are based on the cost of investment of its components. Several

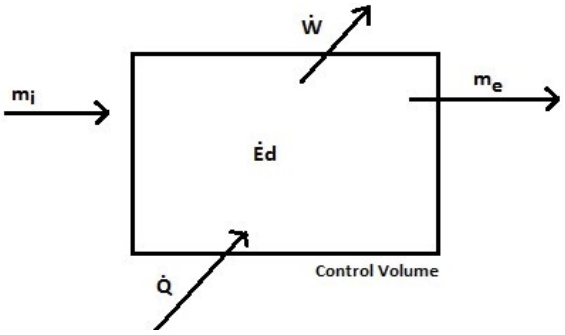

Fig. 3. Control volume.

methods have been proposed to determine the cost of purchasing equipment based on the terms of design parameters. Here, we use the cost function proposed by Rosen and Dincer [28]. However, changes have been made in order to achieve regional conditions in Iran. To convert the cost of investment into cost per unit time, one can write:

$$\dot{Z}_k = \frac{Z_k \times \mathrm{CRF} \times \varphi}{\left(N \times 3{,}600\right)} \tag{5}$$

where Z_k is the cost of purchasing equipment in dollars. The cost-return factor (CRF) in this relationship depends on the estimated interest rate and estimated lifetime for equipment. CRF is calculated according to Eq. (6) [31–34]:

$$\mathrm{CRF} = \frac{i \times \left(1+i\right)^n}{\left(1+i\right)^n - 1} \tag{6}$$

where i is the interest rate and n is the sum of years of operation of the system [35]. In Eq. (5), N represents the number of hours of operation of the CPWSC in 1 y, and Φ the maintenance factor, which are respectively 7,446 and 1.06.

To calculate the cost of exergy in each streamline, the cost balance equation is written separately for each component of the CPWSC. There are many approaches in this field. In this study, the specific exergy costing (SPECO) method is used [18,25]. This method is based on the specific exergy and the cost of each exergy unit and the auxiliary cost equations for each component of the thermal system. This method consists of three steps: the first step, the identification of the exergy flow. The second step is to define the fuel and product for each component of the CPWSC. Step three is to write the cost equation for each component.

Accordingly, the cost balance equation is written for the k-th component of the CPWSC based on the following relation [36,37]:

$$\sum\left(c_{\mathrm{in}}\dot{\mathrm{E}}\mathrm{x}_{\mathrm{in}}\right)_k + c_{w,k}\dot{w}_k = \sum\left(c_{\mathrm{out}}\dot{\mathrm{E}}\mathrm{x}_{\mathrm{out}}\right)_k + c_{\mathrm{heat},k}\dot{\mathrm{E}}\mathrm{x}_{\mathrm{heat},k} + \dot{Z}_k \tag{7}$$

Eq. (7) is written using cost balance equations and auxiliary equations separately for each component [18,38].

In the cost balance Eq. (11), there is no cost term that directly correlates with the exergy destruction of components. Accordingly, the cost associated with the exergy destruction in a component or process will be hidden cost, which will only appear in the thermo-economic analysis. The effect of exergy destruction will appear with the combination of the exergy balance Eq. (8) and economic exergy balance Eq. (9):

$$\dot{\mathrm{E}}\mathrm{x}_{F,k} = \dot{\mathrm{E}}\mathrm{x}_{P,k} + \dot{\mathrm{E}}\mathrm{x}_{L,k} + \dot{\mathrm{E}}\mathrm{x}_{D,k} \tag{8}$$

$$c_{P,k}\dot{\mathrm{E}}\mathrm{x}_{P,k} = c_{F,k}\dot{\mathrm{E}}\mathrm{x}_{F,k} - \dot{C}_{L,k} + \dot{Z}_k \tag{9}$$

where $\dot{C}_{L,k}$ is the cost rates associated with exergy loss that represents the monetary loss associated with the rejection of exergy from a system to its surrounding [25]. As is clear from the above equations, the exergy loss cost rate ($\dot{C}_{L,k}$) affects the product cost rate ($\dot{C}_{P,k}$).

By eliminating $\dot{\mathrm{E}}\mathrm{x}_{F,k}$ from the above equations, the following equation will be obtained:

$$c_{P,k}\dot{\mathrm{E}}\mathrm{x}_{P,k} = c_{F,k}\dot{\mathrm{E}}\mathrm{x}_{P,k} + \left(c_{F,k}\dot{\mathrm{E}}\mathrm{x}_{L,k} - \dot{C}_{L,k}\right) + \dot{Z}_k + c_{F,k}\dot{\mathrm{E}}\mathrm{x}_{D,k} \tag{10}$$

And by eliminating $\dot{\mathrm{E}}\mathrm{x}_{P,k}$, the following relation is obtained:

$$c_{P,k}\dot{\mathrm{E}}\mathrm{x}_{F,k} = c_{F,k}\dot{\mathrm{E}}\mathrm{x}_{F,k} + \left(c_{P,k}\dot{\mathrm{E}}\mathrm{x}_{L,k} - \dot{C}_{L,k}\right) + \dot{Z}_k + c_{P,k}\dot{\mathrm{E}}\mathrm{x}_{D,k} \tag{11}$$

Since the purpose of these calculations is to obtain the costs of the final products, so $\dot{C}_{L,k} = 0$ is considered.

The last term on the right of Eqs. (10) and (11) will include the exergy destruction rate. As discussed earlier, assuming that the product exergy is constant and the cost of the fuel unit $\dot{C}_{F,k}$ for the k-component is independent of the exergy destruction, the cost of the exergy degradation is defined by the last term of Eq. (10) [25].

$$\dot{C}_{D,k} = c_{F,k}\dot{\mathrm{E}}\mathrm{x}_{D,k} \tag{12}$$

One of the goals of this study is to reduce CO_2 emissions. The CO_2 generation in the combustion chamber is due to the combustion reaction, which is related to various properties, including the adiabatic temperature of the flame. The adiabatic flame temperature can be calculated from the following equation [37,39,40].

$$T_{\mathrm{pz}} = A\sigma^{\alpha}\exp\left(\beta\left(\sigma+\lambda\right)^2\right)\pi^{x^*}\theta^{y^*}\xi^{z^*} \tag{13}$$

Table 1
Design specifications of Abadan power plant

Cooling tower temperature difference	45	Design temperature (°C)	26
Power generation (MW)	450	Elevation (m)	3
Humidity (%)	44	Condenser pressure (Kpa)	9

$$\dot{m}_{CO_2} = 44.01 \times x \times \left(\frac{\dot{m}_{fuel}}{m_{fuel}} \right) \quad (14)$$

where x is the molar ratio of carbon in the fuel and m_{fuel} is the molar mass of fuel. This simple equation estimates precisely the CO_2 emission rate in the complete combustion process.

We now investigate the thermodynamic model of a multi-effect steam water desalination cycle, which is located at the condenser site of the CPWSC which is seen in Fig. 2. The equilibrium equations of each effect have been specified in Eqs. (15)–(24). For each effect, the mass and energy conservation are considered in accordance with the control volume (Fig. 4) [6].

Water mass balance in effect *i*:

$$F_i + B_{i-1} = D_i + B_i \quad (15)$$

Brine balance in *i*-th effect:

$$F_i X_{F_i} + X_{B_{i-1}} B_{i-1} = X_{B_i} B_i \quad (16)$$

In Eqs. (15) and (16), *F*, *B*, and *D*, respectively, represent the mass flow rates of feed water, saline water, and non-saline steam (distilled water), and the *F* and *B* indices also indicate feed water and saline water. The concentration of saline water exiting from the system is obtained from Eq. (17) [6]:

$$X_b = 0.9\left(457,628.5 - 1,304.11T_b + 107.5781T_b^3 - 0.360747T_b^3\right) \quad (17)$$

In (17), the parameter X_b represents the concentration of saline water of the effect *i* in mg/L. In this regard, the maximum concentration for drainage water was 70,000 mg/L.

Energy balance of the effect *i*:

$$D_{i-1}\lambda_{i-1} + d_{i-1}\lambda_{i-1} + d'_{i-1}\lambda'_{i-1} = F_i C_p \left(T_i - T_f\right) + D_i\lambda_i \quad (18)$$

In Eq. (18), *d* is the amount of steam formed by the evaporation of the saline water entering the previous stage, *d'* is the water steam content formed by the evaporation of water in a sudden evaporation chambers, λ represents latent heat, C_p is the specific heat in constant pressure, and T_i represents the boiling temperature. The first and the second terms on the left side of Eq. (18) are true from effect 2 to the next, and the third sentence is true from effect 3 onwards. The value of C_p depends on the concentration of feed water and its temperature. The value of latent heat only depends on temperature. The steam temperature formed in the *i*-th stage:

$$T_{vi} = T_i - \text{BPE} \quad (19)$$

In Eq. (19), BPE represents the boiling temperature increase due to the presence of salt within it and the range of this value is between 0.8 and 1.2. T_{vi} is the steam formed from feed water boiling.

$$T_{c,i} = T_i - \text{BPE} - \Delta T_{dem} - \Delta T_{tr} - \Delta T_c \quad (20)$$

In Eq. (20), $T_{c,i}$ is the condensation temperature of steam in the pipes of the next effect and is lower than the boiling temperature of the steam in the previous effect by the sum of the BPE and the losses due to the pressure drop in the dewatering (ΔT_{dem}), the friction of the transmission lines (ΔT_{tr}), and the losses during the condensation (ΔT_c).

The steam formed by the evaporation of saline water in the effect [6]:

$$d_i = B_{i-1} C_p \frac{T_{i-1} - T'_i}{\lambda_i} \quad (21)$$

where

$$T'_i = T_i + \text{NEA}_{\text{BrineFlash}} \quad (22)$$

In Eq. (22), T'_i is the temperature of the saline water removed from the previous stage entering a new stage for cooling. λ_i is the latent heat at the steam temperature of the effect calculated (T_{vi}) and the NEA_j is the non-equilibrium allowance range calculated from Eq. (23). In this relationship, the temperatures are in °C:

$$\left(\text{NEA}\right)_{\text{BrineFlash}} = \frac{0.33\left(T_{i-1} - T_i\right)^{0.55}}{T_{vi}} \quad (23)$$

The thermodynamics of the parabolic solar collector cycle, which acts at the high pressure of the HRSG, has been studied. A parabolic solar collector has been used in the power plant, as shown in Fig. 5. Also, a section of the absorption tube has been shown in the following figure and, its various layers are identified. The geographical specifications of the research site have been shown in Table 2.

θ is the angle between the solar radiation and the normal vector of collector plates to place parabolic solar collectors in the north-south direction [7,8,41].

$$\cos\theta = \sin\varphi\sin\delta\cos\beta + \cos\varphi\cos\delta\cos\omega\cos\beta + \cos\delta\sin\omega\sin\beta \quad (24)$$

The thermal power obtained by the parabolic solar collector is obtained from Eq. (25) [6,41].

$$\dot{Q}_l = I_b A_a \cos\theta N \quad (25)$$

In Eq. (25) A_a is the area of the collector plate, and the maximum value of $\bar{I}_b\cos\theta$ occurs in the early summer.

$$A_a = \left(W - D_{co}\right)L \quad (26)$$

Table 2
Geographical specifications of the CPWSC

Design point parameter	Value
Latitude, °	30.22
Longitude, °	48.20
Location	Abadan

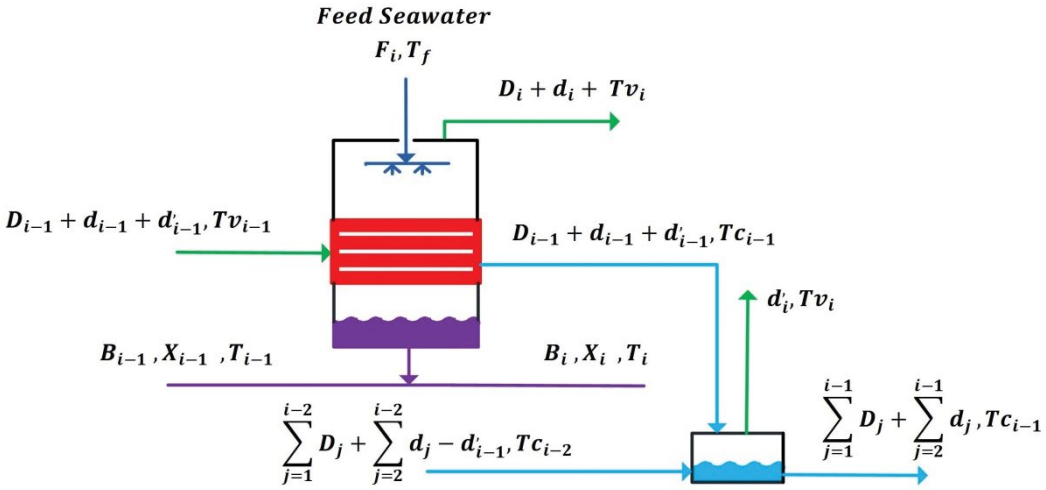

Fig. 4. Schematic view of one of the effects in MED system [6].

where W is the collector plate width, L is the length of the plate, and D_{co} is the outer diameter of the absorber collector cover. The thermal power absorbed by the absorbent is obtained from Eq. (27) [7,8,41].

$$\dot{Q}_a = I_b \cdot A_a \cdot \mathrm{IAM} \cdot N \cdot \gamma_s \cdot \tau_g \cdot \alpha_a \cdot \mathrm{IF} \cdot \eta_{sd} \cdot \mathrm{EL} \tag{27}$$

where γ_s represents the reflection coefficient of the reflector, τ_g is the transmission coefficient of the glass cover of the absorbent pipe, α_a is the absorptivity of absorber, IF is intercept factor, η_{sd} represents the coefficient of correction of the effect of shading caused by dust and EL coefficient of power loss, and their values have been given in Table 3. IAM as the coefficient of the solar radiation angle optimizer for parabolic solar collectors is obtained by Eq. (28) [39].

$$\mathrm{IAM} = \cos\theta - 2.859621\times10^{-5}\times(\theta)^2 - 5.25097\times10^{-4}\times(\theta) \tag{28}$$

$$\mathrm{EL} = 1 - \frac{f}{L}\tan\theta \tag{29}$$

The thermal power $\dot{Q}_u$ from the heat transfer fluid is calculated from the following equation [41]:

$$\dot{Q}_u = F_r - \left(\dot{Q}_a - U_l A_r \left(T_i - T_e\right)\right) \tag{30}$$

$$\dot{Q}_u = m_f C_{pf}\left(T_e - T_i\right) \tag{31}$$

$$A_r = \pi D_i L \tag{32}$$

F_r as the heat loss factor of collector is obtained for each part of the collector through the following equation:

$$F_r = \frac{m_f C_p}{U_L A_r}\left(1 - e^{-\left(\frac{U_L A_r F'}{m_f C_p}\right)}\right) \tag{33}$$

The efficiency of the collector is calculated from the following equation [46].

$$F' = \frac{1}{U_L}\left(\frac{1}{U_L} + \frac{D_o}{D_i h_f} + \frac{D_o}{2k_r}\ln\left(\frac{D_o}{D_i}\right)\right) \tag{34}$$

The heat loss coefficient for different values of absorbent temperature is obtained by using Eqs. (35)–(38) with the initial and repeated guess which corresponds to the section shown in Fig. 5 [41].

$$\dot{Q}_l = \pi U_l D_o \left(T_r - T_o\right) L \tag{35}$$

$$q_{\mathrm{loss}} = q_{c-s} = \pi D_{co} h_w \left(T_{co} - T_o\right) + \pi\sigma D_{co}\varepsilon_c\left(T_{co}^4 - T_{\mathrm{sky}}^4\right) \tag{36}$$

$$q_{\mathrm{loss}} = q_{c-c} = \frac{2\pi k_c \left(T_{ci} - T_{co}\right)}{\ln\left(D_{co}/D_{ci}\right)} \tag{37}$$

$$q_{\mathrm{loss}} = q_{r-c} = \pi D_o \sigma\left(T_r^4 - T_{ci}^4\right)/\left(\frac{1}{\varepsilon_r} + \frac{D_o}{D_{ci}}\left(\frac{1}{\varepsilon_c} - 1\right)\right) \tag{38}$$

In this section, the following relationships are used to calculate the variables of the CPWSC. Eq. (29) provides the exergy efficiency of the CPWSC where, $\mathrm{E\dot{x}}_{Q_h}$ and $\mathrm{E\dot{x}}_{Q_c}$ are the exergy due to the absorbed heat in the parabolic solar collector cycle by the sun and MED system [41–43].

$$\eta_{\mathrm{ex}} = \frac{\left(\sum_n \dot{W}_n\right) + \mathrm{E\dot{x}}_{Q_h} + \mathrm{E\dot{x}}_{Q_c}}{\mathrm{E\dot{x}}_f} \tag{39}$$

Eq. (40) is the sum of the costs of the components of the CPWSC, the cost of fuel used in the combustion chamber, the fire channel, and the cost associated with the exergy destruction.

Table 3
Optical characteristics of parabolic solar collector [41]

Absorber tube outer diameter	0.07	M
Absorber tube inner diameter	0.055	M
Glass envelope outer diameter	0.115	M
Glass envelope inner diameter	0.109	M
Number of modules per collector	8	–
Number of collectors in a loop	8	–
Length of every module	12.27	M
Focal length	1.71	M
Aperture width	5.77	M
Intercept factor	0.92	–
Mirror reflectivity	0.92	–
Glass transmissivity	0.945	–
Solar absorptivity	094	–
Losses due to shading of heat collector element by dust on the envelope	0.98	–

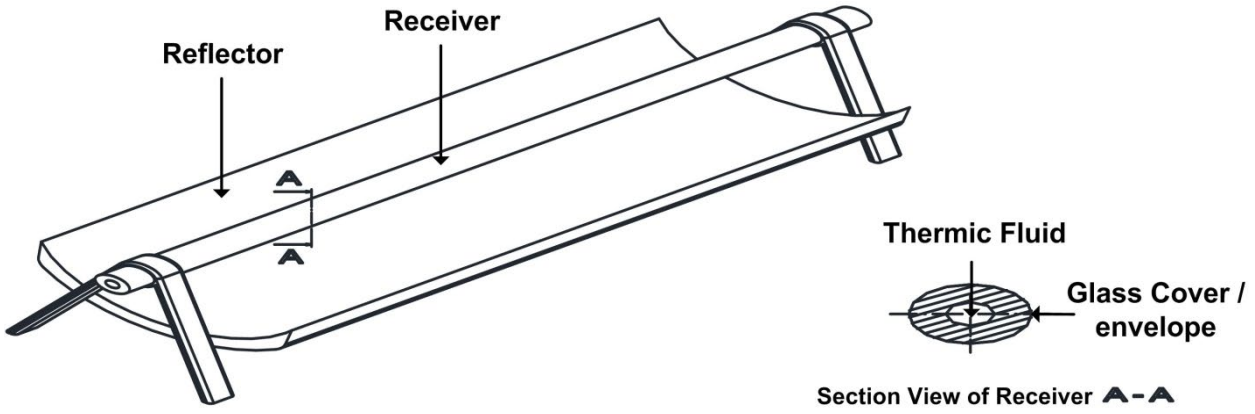

Fig. 5. Parabolic solar collector and absorption tube [41].

$$\dot{C}_{\text{Total}} = \dot{C}_F + \sum_k \dot{Z}_k + \dot{C}_{\text{Env}} + \dot{C}_D \tag{40}$$

$$\dot{C}_{\text{Env}} = c_{\text{NO}_x}\dot{m}_{\text{NO}_x} + c_{\text{CO}_2}\dot{m}_{\text{CO}_2} \tag{41}$$

$$\dot{C}_F = c_f \dot{m}_f \times \text{LHV} \tag{42}$$

Eq. (43) represents the CO_2 emission rate by the CPWSC, which is calculated from the following equation. $\dot{Q}_h$ and $\dot{Q}_c$ are the energy generated by the absorbed heat in the parabolic solar collector cycle by the sun and MED system [8].

$$\in = \frac{\dot{m}_{\text{CO}_2}}{\dot{W}_{\text{net}} + \dot{Q}_h + \dot{Q}_c} \tag{43}$$

3. Discussion

First, for the validation of thermodynamic modeling of Abadan power plant, the results of modeling and system design conditions have been compared in Table 4.

As shown in Table 4, the modeling performed in this study is in good agreement with the design information of the system. In the following, the results of the addition of MED system and parabolic solar collector have been investigated and analyzed.

The results of the performance of various parameters of the CPWSC have been presented in Table 5. The thermal efficiencies of the Abadan CCPP and the CPWSC are 48.71 and 50.91 respectively. The amount of freshwater produced by the CPWSC with 6 evaporation effects is 20,000 ton/d.

The results of the exergy analysis, which include the amount of exergy destruction in various components of the CPWSC, have been shown in Fig. 6. In this figure, it is observed that the highest rate of exergy destruction occurs in the combustion chamber at 200 MW that, this is due to the irreversibility caused by the combustion process and the higher temperature difference between the air entering the combustion chamber and the flame temperature in this chamber.

In accordance with Fig. 6, the condenser is another component of the CPWSC with higher exergy degradation than other constituents. The resulting destruction rate is

Table 4
Validation of thermodynamic modeling of Abadan power plant and system design conditions

State point	This study		Design condition		Deviation	
	T (K)	*P* (kpa)	*T* (K)	*P* (kpa)	*T* (%)	*P* (%)
1	288.15	102.6	288.15	102.6	0.00	0.00
2	595.223	1,026	595.1	1,023	0.016	0.29
3	1,323.2	999.7883	1,323.2	998.2	0.00	0.16
4	817.966	102.6	816.15	98.89	0.22	3.75
5	724.397	102.6	720.6	99.1	0.52	3.53
6	590.57	102.6	592.4	99.26	–0.31	3.36
7	512.29	102.6	513.7	99.52	–0.28	3.10
8	510.05	102.6	510.5	99.88	–0.09	2.72
9	469.29	102.6	468.9	99.98	0.08	2.62
10	423.87	102.6	423.3	100.2	0.136	2.43
11	412.75	102.6	411.9	100.3	0.205	2.34
12	374.636	102.6	374.2	100.4	0.105	2.15
25	317.54	9.3	320	9	–0.78	3.33
26	317.55	9.3	318.9	9.15	–0.43	1.96
27	317.55	105.4	315.6	101.7	0.625	3.6
30	373.15	105.4	372.5	105	0.173	0.4
40	374.15	945.9	374.10	936.8	0.013	0.97
42	439.29	742.63	439.2	715.4	0.01	3.8
44	439.29	721	439.2	721.4	0.01	–0.05
48	441.26	8,147	442.7	8,102	–0.32	0.55
50	565.57	7,925	565.2	7,638	0.066	3.76
51	565.57	7,710	565.6	7,462	–0.006	3.33
62	488.15	700	486.7	696	0.307	0.57

Table 5
Comparison of the specifications of Abadan power plant and CPWSC

Parameters	Co-generation with parabolic solar collector	Combine cycle	Units
Heat input to CC	752.40	752.40	MW
Solar power incident on the collectors	17,868.8	–	KW_{th}
Maximum value of DNI	822.79	–	W/m^2
Actual aperture area	21,714.1	–	M^2
Power output	455.99	444.6	MW
Heat input to cycle	3,038,900	2,998,100	MWh
Fuel mass flow rate	9.8152	9.8152	Kg/s
Plant energy efficiency	50.91	48.71	%
Plant exergy efficiency	50.03	45.91	%
Environmental effect of CO_2	54.97	58.05	Kg/MWh
Distilled water	20,000	–	ton/d

40 MW that, the main reason is the difference in temperature between the two steam and water and the high pressure drop in the condenser. The heat loss in the steam cycle is reduced by 29% and the reduction of 13.56% in the cost of exergy destruction is observed in the condenser.

With the addition of multi-effect desalination to the plant and the production of 20,000 tons per day of freshwater, with the sale rate of $0.16 per cubic meter in Iran, the income from the sale of fresh water to the cogeneration plant $0.037 per second for the power plant.

The economical thermodynamic information of the CPWSC for each component is presented in Table 6, which includes the exergy destruction, the cost of exergy destruction, the cost of fuel exergy, the cost of investment, and total.

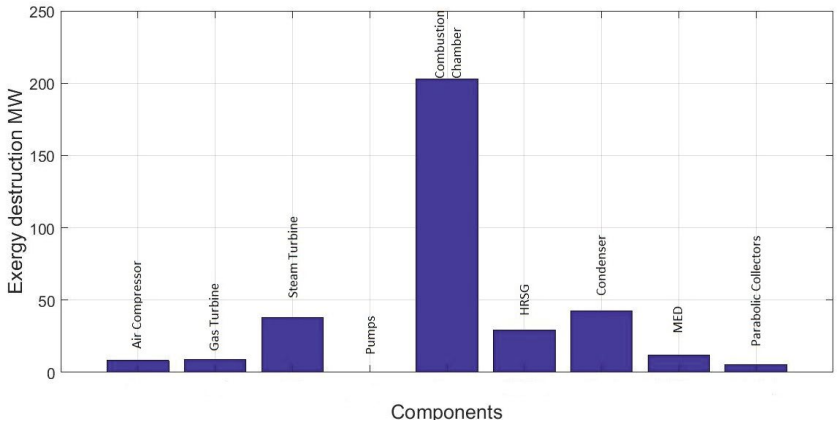

Fig. 6. Results of exergy destruction in various components of the CPWSC.

Table 6
Economic characteristics of the CPWSC

Component	$\dot{Z}+\dot{C}_D$	$\dot{Z}\left(\frac{\$}{s}\right)$	$\dot{C}_F\left(\frac{\$}{s}\right)$	$\dot{C}_D\left(\frac{\$}{s}\right)$	$\dot{E}_D\left(\frac{kj}{s}\right)$
Compressor	0.2217	0.0885	2.2901	0.1332	7.1016e3
Combustion chamber	1.2128	0.0047	3.7446	1.2135	1.7329e9
Gas turbine	0.093	0.0179	2.6224	0.0754	7.4376e6
HRSG	0.3835	0.1381	1.1965	0.2454	3.0378e4
Condenser	0.0198	0.0106	0.0094	0.0091	3.7333e4
BFP pumps	0.0040	0.0040	0.0126	2.9499e-17	2.8816e-12
Steam turbine	2.1278	1.886	1.3455	0.2390	3.4126e4
MED	0.2325	0.2164	0.0820	0.0162	1.0915e4
Parabolic solar collectors	0.4310	0.0571	0.5106	0.1743	1.2183e4

In Fig. 7, the effect of pressure ratio on the exergy efficiency of Abadan plant and the same power plant once with parabolic solar collector and again with MED system has been investigated. As can be seen from Fig. 7, adding a parabolic solar collector at the pressure ratio of 11, and by adding MED system, the exergy efficiency of the Abadan power plant increases by approximately 2% and 4.2% respectively. In other words, the compressor pressure ratio change rate does not affect the slope of exergy efficiency in three modes of CCPP and CPWSC and cogeneration power and water plant (CPWP). This diagram shows for CPWP, higher exergy efficiency increase can be obtained compared to adding parabolic solar collectors. Because in parabolic solar collectors, the share of exergy losses is high and hence they have a smaller share in increasing the exergy efficiency.

Fig. 8 shows the changes in the cost of exergy destruction of the CPWSC versus increasing the temperature of gas entering the gas turbine for the pressure ratios of 10, 12, and 14. By increasing the temperature of the gas entering the gas turbine from 1,260 to 1,550 K at a pressure ratio of 10, 12, and 14, the exergy destruction cost decreases by 25%, 50%, and 60% respectively, also, according to Fig. 8, with increasing compressor pressure ratio, the cost of total exergy destruction increases. According to Fig. 9, with an increase in freshwater production from 100 to 350 kg/s, with 7 effects on the

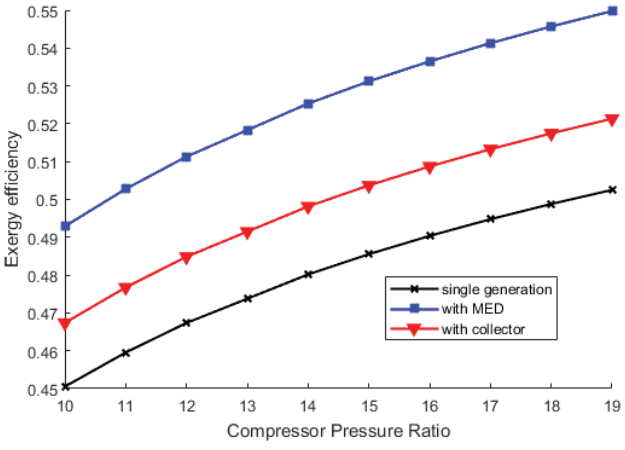

Fig. 7. Compressor pressure ratio variations versus exergy efficiency.

CPWSC, the exergy efficiency increases by 0.1. Similarly, for 8 effects, the exergy efficiency increases. But in 6 effects, with increasing water production, the exergy efficiency is increasing and decreasing. Also, increasing the number of effects reduces the efficiency of exergy.

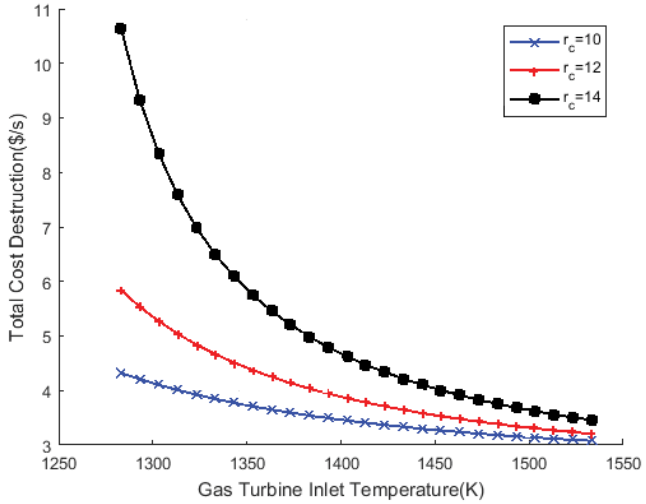

Fig. 8. Exergy degradation cost changes by increasing the temperature of gas entering the gas turbine.

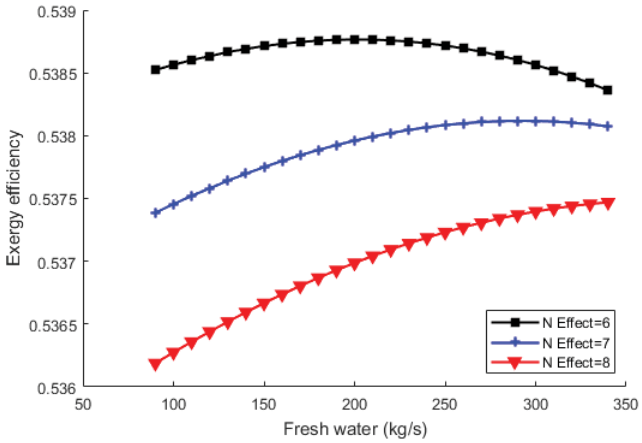

Fig. 9. Freshwater production and the number of effects on the exergy efficiency of the CPWSC.

According to Fig. 10, by increasing the production of freshwater from 100 to 350 kg/s, the production cost per megawatt hour of electricity can be reduced by 30%. However, with the increase in the number of effects, the cost of electricity generation increases by 0.2 cents per megawatt hour. In Fig. 11, considering the investment cost and the cost of exergy losses and the cost of emissions, it can be seen from the graph that, with the increase in the lifetime of the CPWSC, the cost of electricity generation per megawatt hour during 30 y of the operation of the CPWSC will be reduced by about 50%. Also, with 20 y of power plant life, the cost of electricity and water will reach the stable status. Of course, it is observed that by changing the profit rate from 10% to 14% in the first 5 y of the activity of the CPWSC, electricity costs are not significantly different but over time, the cost of electricity generation can be reduced by reducing the profit rate.

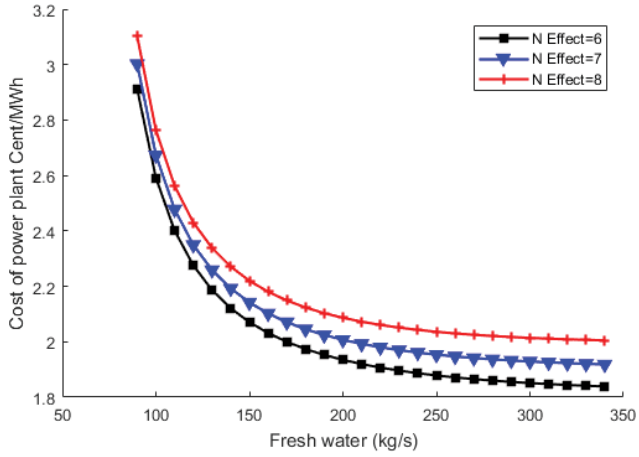

Fig. 10. Effect of fresh water production on the cost of electricity generation at the CPWSC.

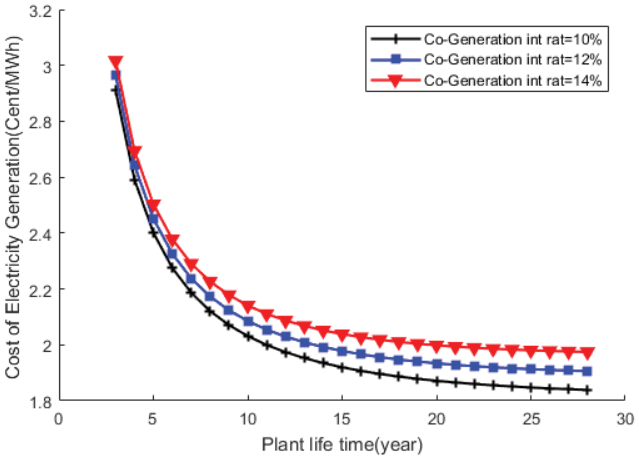

Fig. 11. Comparison of the lifetime of the CPWSC and the cost of generating electricity plus the production profit percentage.

Fig. 12 shows the cost of electricity generation at a profit rate of 10% during the 30 y period of operation of the CPWSC vs. to the Abadan CCPP to be about 0.3 cent/MWh higher. Fig. 13 shows the variation in the environmental impact and the compressor pressure ratio. It can be seen that by adding a parabolic solar collector and MED system to Abadan CCPP, the pollution from power plant decreased by 4% in the ratio of 10–35. Also, at the pressure ratio of 11, where Abadan power plant performs better at this pressure ratio, the decrease in the environmental impact caused by adding a parabolic solar collector and MED system is about 2.

4. Conclusion

This research has provided the use of the well-known method of economical thermodynamic analysis of SPECO in order to evaluate the CPWSC. Economical exergy variables, cost equilibrium equations, and auxiliary equations for each component of the CPWSC have been obtained and the

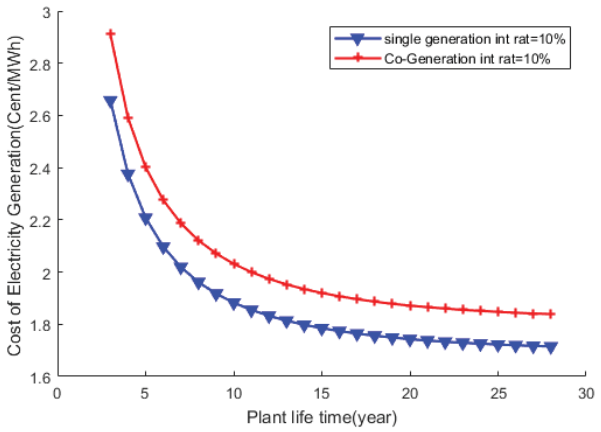

Fig. 12. Comparison of the cost of electricity generation between Abadan power plant and the CPWSC.

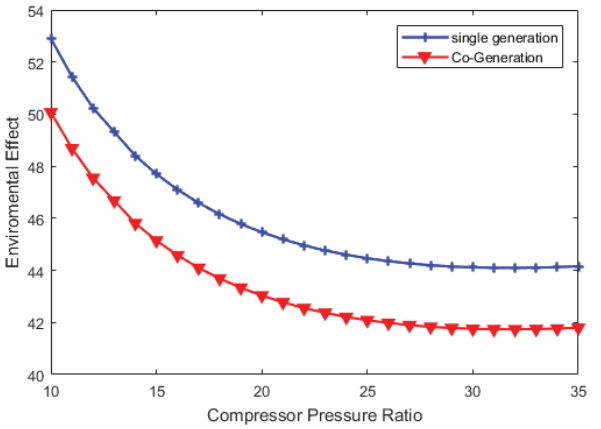

Fig. 13. Changes in the environmental impact and compressor pressure ratio.

average cost of each exergy unit for different points has been calculated by solving the equation system.

The main conclusions reached in this study are the following:

- By applying changes, including employs six evaporation effects and parabolic solar collectors, in a CCPP, in addition to producing 20,000 tons of freshwater daily, the amount of heat loss 29% in the steam cycle and the cost rate of exergy destruction 13.56% in the condenser is reduced.
- By increasing the amount of freshwater produced with constant investment cost, the cost of electricity generation of the CPWSC could be reduced by 36%. The cost of electricity generation with a profit rate of 10% over the course of 30 y of the operation of CPWSC has been compared with Abadan CCPP that, higher costs of about 0.3 cents per megawatt hour of electricity are observed. However, in contrast, the thermal efficiency, and exergy efficiency of the Abadan CCPP with the addition of MED system and parabolic solar collector, has increased from 48.71 to 50.91, and from 45.91 to 50.03, respectively.
- At the pressure ratio of 11, which is the design conditions of the Abadan CCPP, the environmental impact caused by adding a parabolic solar collector and MED system decreases by about 2%. On the other hand, CO_2 emissions decreased from 58.05 to 54.97 kg per megawatt hour of electricity.
- According to the provided contents, it can be concluded that, the SPECO economic exergy analysis method is an effective tool for identifying and evaluating inefficiencies in terms of cost and efficiency.

Symbols

c	—	Cost per exergy unit, $/MJ
c_f	—	Cost of fuel per energy unit, $/MJ
$\dot{C}$	—	Cost flow rate, $/s
c_p	—	Specific heat at constant pressure, kJ/kg K
CRF	—	Capital recovery factor
$\dot{E}x$	—	Exergy flow rate, MW
$\dot{E}x_D$	—	Exergy destruction rate, MW
ex	—	Specific exergy, kJ/kg
i	—	Annual interest rate, %
h	—	Specific enthalpy, kJ/kg
h_0	—	Specific enthalpy at environmental state, kJ/kg
LHV	—	Lower heating value, kJ/kg
$\dot{m}$	—	Mass flow rate, kg/s
n	—	Number of years
N	—	Number of hours of plant operation per year
PP	—	Pinch point
$\dot{Q}$	—	Heat transfer rate, kW
r_{AC}	—	Compressor pressure ratio
s	—	Specific entropy, kJ/kg K
s_0	—	Specific entropy at environmental state, kJ/kg K
$\dot{W}_{net}$	—	Net power output, MW
Z	—	Capital cost of a component, $
$\dot{Z}$	—	Capital cost rate, $/s

Greek letters

η	—	Isentropic efficiency
ξ	—	Coefficient of fuel chemical exergy
Φ	—	Maintenance factor

Subscripts

a	—	Air
AC	—	Air compressor
CC	—	Combustion chamber
CCPP	—	combined cycle power plant
ch	—	Chemical
Cond	—	Condenser
CPWSC	—	Cogeneration of Power and Water with the parabolic solar collectors
GT	—	Gas turbine
HP	—	High pressure
HRSG	—	Heat recovery steam generator
ST	—	Steam turbine
LP	—	Low pressure
ph	—	Physical

w	—	Water
TVC	—	Thermal vapor compression
MSF	—	Multi-stage flash
MED	—	Multi-effect distillation
SWRO	—	Sea water reverse osmosis
IAM	—	Incidence angle modifier

References

[1] R. Loni, A.B. Kasaeian, O. Mahian, A.Z. Sahin, Thermodynamic analysis of an organic rankine cycle using a tubular solar cavity receiver, Energy Convers. Manage., 127 (2016) 494–503.

[2] O. Mahian, A. Kianifar, A.Z. Sahin, S. Wongwises, Entropy generation during Al_2O_3/water nanofluid flow in a solar collector: effects of tube roughness, nanoparticle size, and different thermophysical models, Int. J. Heat Mass Transfer, 78 (2014) 64–75.

[3] M.A. Sabiha, R. Saidur, S. Mekhilef, O. Mahian, Progress and latest developments of evacuated tube solar collectors, Renewable Sustainable Energy Rev., 51 (2015) 1038–1054.

[4] S. Dabiri, E. Khodabandeh, A.K. Poorfar, R. Mashayekhi, D. Toghraie, S.A.A. Zade, Parametric investigation of thermal characteristic in trapezoidal cavity receiver for a linear Fresnel solar collector concentrator, Energy, 153 (2018) 17–26.

[5] E. Khodabandeh, M.R. Safaei, S. Akbari, O.A. Akbari, A.A.A.A. Alrashed, Application of nanofluid to improve the thermal performance of horizontal spiral coil utilized in solar ponds: geometric study, Renewable Energy, 122 (2018) 1–16.

[6] I.S. Al-Mutaz, I. Wazeer, Development of a steady-state mathematical model for MEE-TVC desalination plants, Desalination, 351 (2014) 9–18.

[7] A. Baghernejad, M. Yaghoubi, Exergy analysis of an integrated solar combined cycle system, Renewable Energy, 35 (2010) 2157–2164.

[8] A. Baghernejad, M. Yaghoubi, K. Jafarpur, Exergoeconomic optimization and environmental analysis of a novel solar-trigeneration system for heating, cooling and power production purpose, Sol. Energy, 134 (2016) 165–179.

[9] Y. Sanjay, O. Singh, B.N. Prasad, Energy and exergy analysis of steam cooled reheat gas-steam combined cycle, Appl. Therm. Eng., 27 (2007) 2779–2790.

[10] S. Ihm, O.Y. Al-Najdi, O.A. Hamed, G. Jun, H. Chung, Energy cost comparison between MSF, MED and SWRO: case studies for dual purpose plants, Desalination, 397 (2016) 116–125.

[11] N. Si, Z. Zhao, S. Su, P. Han, Z. Sun, J. Xu, X. Cui, S. Hu, Y. Wang, L. Jiang, Exergy analysis of a 1000 MW double reheat ultra-supercritical power plant, Energy Convers. Manage., 147 (2017) 155–165.

[12] A.A.A. Abuelnuor, K.M. Saqr, S.A.A. Mohieldein, K.A. Dafallah, M.M. Abdullah, Y.A.M. Nogoud, Exergy analysis of Garri "2" 180 MW combined cycle power plant, Renewable Sustainable Energy Rev., 79 (2017) 960–969.

[13] M.A. Lozano, A. Valero, Theory of the exergetic cost, Energy, 18 (1993) 939–960.

[14] B. Erlach, L. Serra, A. Valero, Structural theory as standard for thermoeconomics, Energy Convers. Manage., 40 (1999) 1627–1649.

[15] C.A. Frangopoulos, Thermo-economic functional analysis and optimization, Energy, 12 (1987) 563–571.

[16] C.A. Frangopoulos, Intelligent functional approach; A method for analysis and optimal synthesis-design-operation of complex systems, Int. J. Energy Environ. Econ., 1 (1991) 267–274.

[17] G. Tsatsaronis, L. Lin, J. Pisa, Exergy costing in exergoeconomics, J. Energy Resour. Technol., 115 (1993) 9–16.

[18] A. Lazzaretto, G. Tsatsaronis, SPECO: a systematic and general methodology for calculating efficiencies and costs in thermal systems, Energy, 31 (2006) 1257–1289.

[19] M.R. Von Spakovsky, R.B. Evans, Engineering functional analysis—Part I, J. Energy Resour. Technol., 115 (1993) 86–92.

[20] M.R. Von Spakovsky, Application of engineering functional analysis to the analysis and optimization of the CGAM problem, Energy, 19 (1994) 343–364.

[21] M.A. Rosen, I. Dincer, Thermoeconomic analysis of power plants: an application to a coal fired electrical generating station, Energy Convers. Manage., 44 (2003) 2743–2761.

[22] T.J. Kotas, The Exergy Method of Thermal Plant Analysis, Butterworth-Heinemann Publishing, Elsevier, 2013.

[23] M. Ameri, P. Ahmadi, A. Hamidi, Energy, exergy and exergo-economic analysis of a steam power plant: a case study, Int. J. Energy Res., 33 (2009) 499–512.

[24] M.A. Javadi, H. Ghomashi, Thermodynamics analysis and optimization of abadan combined cycle power plant, Indian J. Sci. Technol., 9 (2016) 60–72.

[25] A. Bejan, G. Tsatsaronis, M. Moran, M.J. Moran, Thermal Design and Optimization, Wiley-Interscience Publishing, John Wiley & Sons, 1996.

[26] P. Roosen, S. Uhlenbruck, K. Lucas, Pareto optimization of a combined cycle power system as a decision support tool for trading off investment vs. operating costs, Int. J. Therm. Sci., 42 (2003) 553–560.

[27] S.C. Kaushik, Y.P. Abhyankar, S. Bose, S. Mohan, Exergoeconomic evaluation of a solar thermal power plant, Int. J. Sol. Energy, 21 (2001) 293–314.

[28] M.A. Rosen, I. Dincer, Effect of varying dead-state properties on energy and exergy analyses of thermal systems, Int. J. Therm. Sci., 43 (2004) 121–133.

[29] O. Ozgener, A. Hepbasli, Exergoeconomic analysis of a solar assisted ground-source heat pump greenhouse heating system, Appl. Therm. Eng., 25 (2005) 1459–1471.

[30] M.A. Javadi, S. Hoseinzadeh, M. Khalaji, R. Ghasemiasl, Optimization and analysis of exergy, economic, and environmental of a combined cycle power plant, Sadhana – Acad. Proc. Eng. Sci., 44 (2019) 11–25.

[31] M. Kanoglu, I. Dincer, M.A. Rosen, Understanding energy and exergy efficiencies for improved energy management in power plants, Energy Policy, 35 (2007) 3967–3978.

[32] A.G. Kaviri, M.N.M. Jaafar, Thermodynamic modeling and exergy optimization of a gas turbine power plant, IEEE 3rd International Conference on Communication Software and Networks, Xi'an, China, 2011, pp. 366–370.

[33] P. Ahmadi, I. Dincer, Thermodynamic Analysis and Thermo-economic Optimization of a Dual Pressure Combined Cycle Power Plant with a Supplementary Firing Unit, Energy Convers. Manage., 52 (2011) 2296–2308.

[34] M.A. Javadi, M.H. Ahmadi, M. Khalaji, Exergetic, economic, and environmental analyses of combined cooling and power plants with parabolic solar collector, Environ. Prog. Sustainable Energy, 39 (2019) 10–18.

[35] A. Valero, M.A. Lozano, L. Serra, G. Tsatsaronis, J. Pisa, C. Frangopoulos, M.R. von Spakovsky, CGAM problem: definition and conventional solution, Energy, 19 (1994) 279–286.

[36] J. Szargut, D.R. Morris, F.R. Steward, Exergy Analysis of Thermal, Chemical, and Metallurgical Processes, The University of Michigan, Hemisphere, 1987.

[37] P. Ahmadi, I. Dincer, Exergoenvironmental analysis and optimization of a cogeneration plant system using Multimodal Genetic Algorithm (MGA), Energy, 35 (2010) 5161–5172.

[38] M.A. Javadi, S. Hoseinzadeh, R. Ghasemiasl, P.S. Heyns, A.J. Chamkha, Sensitivity analysis of combined cycle parameters on exergy, economic, and environmental of a power plant, J. Therm. Anal. Calorim., (2019) 519–525, https://doi.org/10.1007/s10973-019-08399-y.

[39] H. Barzegar Avval, P. Ahmadi, A.R. Ghaffarizadeh, M.H. Saidi, Thermo-economic-environmental multiobjective optimization of a gas turbine power plant with preheater using evolutionary algorithm, Int. J. Energy Res., 35 (2011) 389–403.

[40] H. Kariman, S. Hoseinzadeh, S. Heyns, Energetic and exergetic analysis of evaporation desalination system integrated with mechanical vapor recompression circulation, Case Stud. Therm. Eng., 16 (2019) 100548.

[41] S. Adibhatla, S.C. Kaushik, Energy, exergy and economic (3E) analysis of integrated solar direct steam generation combined cycle power plant, Sustainable Energy Technol. Assess., 20 (2017) 88–97.

[42] S.E. Shakib, S.R. Hosseini, M. Amidpour, C. Aghanajafi, Multi-objective optimization of a cogeneration plant for supplying given amount of power and fresh water, Desalination, 286 (2012) 225–234.

[43] S.E. Shakib, M. Amidpour, C. Aghanajafi, Simulation and optimization of multi effect desalination coupled to a gas turbine plant with HRSG consideration, Desalination, 285 (2012) 366–376.